J. Fluid Mech. (1972), *vol.* 55, *part* 2, *pp.* 193–208
Printed in Great Britain

An investigation of particle trajectories in two-phase flow systems

By S. A. MORSI
Department of Mechanical Engineering, University of Surrey
AND A. J. ALEXANDER
Loughborough University of Technology

(Received 12 November 1971)

This paper describes a theoretical investigation into (i) the response of a spherical particle to a one-dimensional fluid flow, (ii) the motion of a spherical particle in a uniform two-dimensional fluid flow about a circular cylinder and (iii) the motion of a particle about a lifting aerofoil section. In all three cases the drag of the particle is allowed to vary with (instantaneous) Reynolds number by using an analytical approximation to the standard experimental drag–Reynolds-number relationship for spherical particles.

1. Introduction

The prediction of particle velocities and trajectories in fluid flow is of a considerable importance in many fields. In studying the erosion damage sustained by nozzles or blades in steam or gas turbines, where these parts are subjected to the flow of a mixture of gas and solids or gas and water drops, Martlew (1960) and Neilson & Gilchrist (1968) have found that the erosion depends on the wall material, the particle velocity and the angle of attack. Similarly, in the design of inertia and impingement filters, the prediction of particle trajectories will be of great help in assessing the efficiency of these filters in capturing solid particles from the carrier fluid.

In the case of flow through a turbine it is desirable for particles not to contact the blades whereas in flow through a filter the opposite effect is needed. In either case it is necessary to know what path a particle will take and although calculations have been made by Langmiur & Blodgett (1946) and Michael & Norey (1969), it is usual to assume that the particle Reynolds number is small and that the Stokes linear approximation to the drag coefficient ($C_d = 24/R_N$) will be valid. This is not always the case and at sufficiently high Reynolds numbers very large errors will result from the use of this formula. In this paper an expression for the drag coefficient which closely approximates to the standard experimental drag–Reynolds-number relationship is used to give an analytical solution in the case of one-dimensional flow and to save computation time in the case of two-dimensional flow.

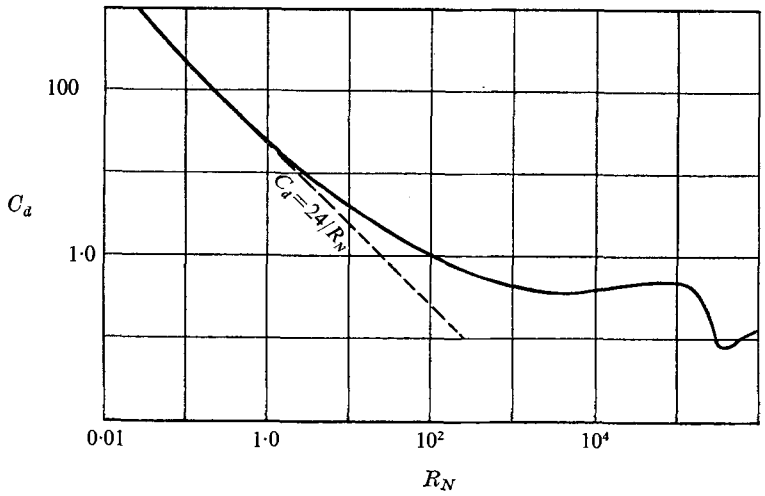

FIGURE 1. Drag coefficient for spherical particles *vs.* Reynolds number.

2. Response of a spherical particle to a one-dimensional fluid flow

When a particle, or a cloud of particles of low concentration, is introduced into an air stream the response of the particle depends on the relative velocity of the particle and the fluid. This relative velocity determines the drag, which is the sole force determining the motion of the particle if it is assumed that there is no particle interaction and further that the presence of the particles does not change the basic flow pattern.

The equation of motion of a single particle is

$$m_p dU_p/dt = C_d \times \tfrac{1}{2}\rho_g (U_g - U_p)^2 A_p, \tag{1}$$

where the subscript p refers to the particle and the subscript g to the gas; A_p is the surface area of the particle. The mass of a spherical particle is given by

$$m_p = \tfrac{1}{6}\pi D_p^3 \rho_p. \tag{2}$$

The drag coefficient C_d for a spherical particle is plotted against the Reynolds number R_N in figure 1. The Reynolds number for a spherical particle is given by

$$R_N = \rho_g (U_g - U_p) D_p/\mu. \tag{3}$$

At very small Reynolds numbers ($R_N \sim 0{\cdot}1$), the flow is known as Stokes flow and under these conditions $C_d = 24/R_N$. Solutions obtained using this condition are given by Zenz & Othmer (1960). At very high Reynolds numbers ($R_N \sim 10^3$) the value of C_d becomes approximately constant at about 0·4, but in the intermediate range of R_N, which is the range of practical interest, C_d varies with R_N in a complicated manner. Many empirical formulae have been suggested but these are suitable only in certain region. In the present paper C_d is calculated at the correct Reynolds number and is always within 1–2 % of the experimental value.

R_N	C_d (experimental)	C_d (calculated)	R_N	C_d (experimental)	C_d (calculated)
0·1	240·0	240·01	100·0	1·07	1·07
0·2	120·0	119·59	200·0	0·77	0·771
0·3	80·0	80·45	300·0	0·65	0·6613
0·5	49·0	49·501	500·0	0·55	0·55
0·7	36·5	36·335	700·0	0·50	0·4991
1·0	26·5	26·503	1000·0	0·46	0·46
2·0	14·4	14·833	2000·0	0·42	0·42
3·0	10·4	10·51	3000·0	0·40	0·4016
5·0	6·9	6·9	5000·0	0·385	0·385
7·0	5·4	5·31	7000·0	0·390	0·391
10·0	4·1	4·1	10 000·0	0·405	0·410
20·0	2·55	2·65	20 000·0	0·45	0·452
30·0	2·00	2·03	30 000·0	0·47	0·4697
50·0	1·50	1·50	50 000·0	0·49	0·488
70·0	1·27	1·257			

TABLE 1. Drag coefficient for spherical particles

In order to obtain this accuracy the experimental drag curve is divided into a number of regions and the curve in that region is approximated to by an equation of the form

$$C_d = \frac{K_1}{R_N} + \frac{K_2}{R_N^2} + K_3. \tag{4}$$

This curve can be made to fit the experimental curve at three points, and the width of the region chosen is adjusted so that the discrepancy between the two curves is negligible, see table 1. The range of Reynolds numbers taken is $0{\cdot}1\text{–}5 \times 10^4$. In the appendix the values of the constants and the drag coefficient equations are given.

The advantage of using (4) is that (1) can be solved analytically and the errors associated with numerical techniques avoided. Equation (1) may be written as

$$dU_p/dt = \phi_1 - \phi_2 U_p + A_1 U_p^2, \tag{5}$$

where

$$\phi_1 = \frac{3\mu K_1 U_g}{4\rho_p D_p^2} + \frac{3\mu^2 K_2}{4\rho_g \rho_p D_p^3} + \frac{3K_3 \rho_g U_g^2}{4D_p \rho_p}, \tag{6}$$

$$\phi_2 = \frac{3\mu K_1}{4\rho_p D_p^2} + \frac{3K_3 \rho_g U_g}{2\rho_p D_p}, \tag{7}$$

$$A_1 = 3K_3 \rho_g / 4D_p \rho_p. \tag{8}$$

Equation (5) is a form of the Riccati equation with constant coefficients if U_g is constant. Under these circumstances an analytic solution can be obtained. For U_g variable the equation can be reduced to the Abel form, in which case an analytic solution can be obtained only for certain types of velocity function.

For constant velocity U_g (5) becomes

$$dU_p/(U_p - \eta_1)(U_p - \eta_2) = A_1 dt, \tag{9}$$

where η_1 and η_2 are the roots of the right-hand side of (5) and are given by

$$\eta_{1,2} = \phi_2/2A_1 \pm [(\phi_2/2A_1)^2 - \phi_1/A_1]^{\frac{1}{2}}. \tag{10}$$

Equation (9) can be solved analytically, and if the particle initial conditions are $U_p = U_{p0}$ and $x = x_0$ when $t = t_0$, then for $\eta_1 = \eta_2$

$$U_p = \eta_1 - \{(U_{p0} - \eta_1)/[A_1(t-t_0)\,(U_{p0} - \eta_1) - 1]\}, \tag{11}$$

for $\eta_1 \neq \eta_2$ and real

$$U_p = \frac{\eta_2 - \{\eta_1(U_{p0} - \eta_2)/(U_{p0} - \eta_1)\} \exp\,[A_1(\eta_2 - \eta_1)\,(t-t_0)]}{1 - \{(U_{p0} - \eta_2)/(U_{p0} - \eta_1)\} \exp\,[A_1(\eta_2 - \eta_1)\,(t-t_0)]} \tag{12}$$

and for $\eta_1 \neq \eta_2$ and imaginary

$$U_p = \frac{\theta U_{p0} + \theta^2 - (\phi_2/2A_1)\,(U_{p0} - \phi_2/2A_1) \tan \theta A_1 (t-t_0)}{\theta - (U_{p0} - \phi_2/2A_1) \tan \theta A_1 (t-t_0)}, \tag{13}$$

where

$$\theta = (\phi_1/A_1) - (\phi_2/2A_1)^2. \tag{14}$$

When the Reynolds number is less than 0·1 equation (9) reduces

$$dU_p/dt = \phi_1 - \phi_2 U_p, \tag{15}$$

and its solution is given by

$$U_p = (\phi_1/\phi_2)\,[1 - e^{-\phi_2(t-t_0)}] + U_{p0} e^{-\phi_2(t-t_0)}. \tag{16}$$

In some cases it is convenient to obtain the distance x travelled by the particle as a function of the velocity. To obtain such relationship, (5) can be rewritten in the following form:

$$U_p\, dU_p/dx = \phi_1 - \phi_2 U_p + A_1 U_p^2. \tag{17}$$

The solution of this equation is

$$x = x_0 + \frac{1}{A_1}\left\{\log\left(\frac{U_p - \eta_1}{U_{p0} - \eta_1}\right) + \frac{\eta_1(U_{p0} - U_p)}{(U_p - \eta_1)\,(U_{p0} - \eta_1)}\right\} \tag{18}$$

for $\eta_1 = \eta_2$,

$$x = x_0 + \frac{1}{A_1}\left\{\frac{\eta_2}{\eta_2 - \eta_1} \log\left(\frac{U_p - \eta_2}{U_{p0} - \eta_2}\right) - \frac{\eta_1}{\eta_2 - \eta_1} \log\left(\frac{U_p - \eta_1}{U_{p0} - \eta_1}\right)\right\} \tag{19}$$

for $\eta_1 \neq \eta_2$

and

$$x = x_0 - \frac{\phi_1}{\phi_2} \log \frac{(\phi_1 - \phi_2 U_p)}{(\phi_1 - \phi_2 U_{p0})} + \frac{1}{\phi_2}(U_p - U_{p0}) \tag{20}$$

for $R_N < 0{\cdot}1$.

In this section a method has been given for obtaining an analytical solution for the equation of motion of a single particle, within any of the regions of Reynolds numbers required, in the horizontal direction. In the case where the actual trajectory of the particle is required, an equation similar to (5) has to be solved for the vertical direction and to include effect of gravity in such equation, the gravitational acceleration g has to be subtracted from the value of ϕ_1.

Figures 2 (*a*) and (*b*) show the change in the particle velocity with the change in the distance x from the particle inlet to an air stream for particles of diameter 50 μm and 100 μm and particle densities of 870 and 1400 kg/m^3.

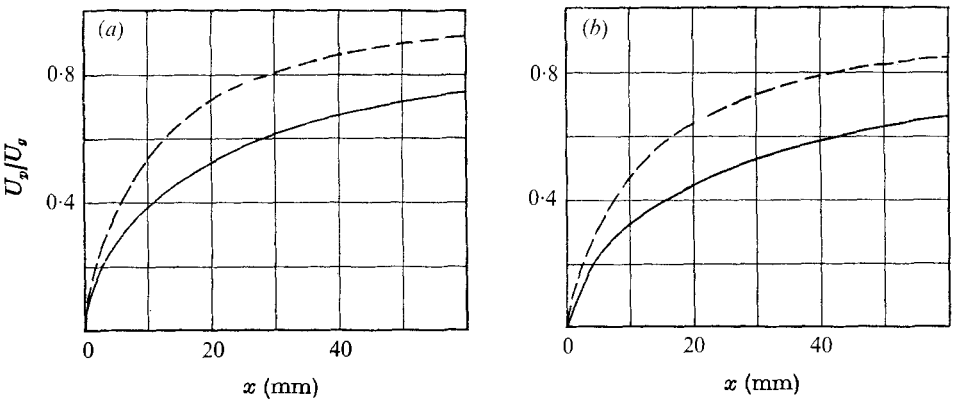

FIGURE 2. Ratio of particle velocity to air velocity *vs.* distance. – – –, $D_p = 50\ \mu$m; ——, $D_p = 100\ \mu$m. (*a*) $\rho_p = 870$ kg/m^3. (*b*) $\rho_p = 1400$ kg/m^3.

3. Collision of spherical particles with a cylinder

Michael & Norey considered the case of particle collision with a sphere and obtained a numerical solution for Stokes flow ($R_N < 0{\cdot}1$). In this paper the case of flow round a circular cylinder is considered but with no restriction on the particle Reynolds number. The equation of motion (1) is used but with a variable velocity U_g obtained from the two-dimensional inviscid flow past a circular cylinder.

The inviscid flow solution for flow past a circular cylinder is well known. In a real flow, separation occurs on the rear of the cylinder but on the upstream half the inviscid solution is a reasonable approximation to the real flow. The velocity field is obtained from the stream function ψ, given by

$$\psi = Uy - Ua^2y/(x^2+y^2), \tag{21}$$

where U is the uniform undisturbed velocity some distance upstream of the cylinder.

The horizontal and vertical velocity components U_g and V_g are given by

$$U_g = \frac{\partial\psi}{\partial y} = U\left(1+\frac{a^2(y^2-x^2)}{(x^2+y^2)^2}\right), \tag{22}$$

$$V_g = -\frac{\partial\psi}{\partial x} = -\frac{2Ua^2xy}{(x^2+y^2)^2}. \tag{23}$$

These satisfy the equation of continuity

$$\partial U_g/\partial x + \partial V_g/\partial y = 0. \tag{24}$$

Apart from the drag force, another force acts on the spherical particles when they move through a velocity gradient. Owing to the difference in velocity, and hence pressure between the top and bottom of the particle when in a velocity gradient, a lift force acts on the particle. The value of the lift coefficient was derived by Saffman (1965) and is given by

$$C_L = 6{\cdot}46\mu D_p^2 R^{\frac{1}{2}}/4\nu^{\frac{1}{2}}, \tag{25}$$

where R is the rate of shear and can be obtained by differentiating (22) and (23). The rate of shear in both directions is identical and is given by

$$R = \left|\frac{dU_g}{dy}\right| = \left|\frac{dV_g}{dx}\right| = \left|\frac{2Ua^2y(3x^2-y^2)}{(x^2+y^2)^3}\right|. \tag{26}$$

Both drag and lift forces are introduced into the equations of motion, which become

$$m_p dU_p/dt = \tfrac{1}{8}C_{dh}\rho_g \pi D_p^2(U_g-U_p)^2 \pm C_L(V_g-V_p), \tag{27}$$

$$m_p dV_p/dt = \tfrac{1}{8}C_{dv}\rho_g \pi D_p^2(V_g-V_p)^2 \pm C_L(U_g-U_p), \tag{28}$$

where the subscripts h and v stand for horizontal and vertical respectively.

Using the appropriate value of C_d from (4) and the value of C_L from (25), equations (27) and (28) become

$$dU_p/dt = \phi_{c1} - \phi_{c2}U_p + A_{c1}U_p^2 \pm F_1 V_p, \tag{29}$$

$$dV_p/dt = \phi_{c11} - \phi_{c22}V_p + A_{c11}V_p^2 \pm F_1 U_p, \tag{30}$$

where

$$\phi_{c1} = \frac{3\mu K_1}{4\rho_p D_p^2}U_g + \frac{3\mu^2 K_2}{4\rho_g\rho_p D_p^3} + \frac{3\rho_g K_3}{4\rho_p D_p}U_g^2 \pm \frac{9{\cdot}69\mu}{\pi\rho_p D_p}\left(\frac{R}{\nu}\right)^{\frac{1}{2}}V_g,$$

$$\phi_{c2} = \frac{3K_1\mu}{4_p D_p} + \frac{3K_3\rho_g}{2\rho_p D_p}U_g,$$

$$A_{c1} = \frac{3K_3\rho_g}{4\rho_p D_p}, \quad F_1 = \frac{6{\cdot}46\mu D_p^2}{4\nu^{\frac{1}{2}}}R^{\frac{1}{2}}.$$

The simultaneous equations (29) and (30) were solved numerically using Runge's method. Three solutions are given in figures 3(*a*)–(*c*) for the following cases. The fluid is air, $D_p = 10\,\mu$m, $20\,\mu$m or $100\,\mu$m, $\rho_p = 1400\,\text{kg/m}^3$, $U = 6\,\text{m/s}$ and the cylinder diameter = 25 mm. The particles were introduced into the flow with zero velocity at a distance of 75 mm from the y axis.

The above examples were solved once more but with the lift force due to the rate of shear excluded (i.e. with $C_L = 0$ in (27) and (28)). The difference between these results and those including the lift force is negligible. Hence the effect of the lift forces is very small compared with that of the drag forces in this range of particle parameters.

4. Collision of spherical particle with a lifting aerofoil

The transformation

$$Z = e^{i\alpha}\left(\zeta - \epsilon l + \frac{l^2}{\zeta-\epsilon l} + \frac{2\epsilon^2 l^2}{a+\epsilon l}\right) \tag{31}$$

will transform a circle of a radius a in the ζ plane to the Joukowsky symmetrical aerofoil in the Z plane (see figure 4). If ϵ is zero then the circle is transformed to a flat plate. On the other hand if ϵ is positive the aerofoil obtained has a thickness proportional to ϵ. A non-symmetrical aerofoil can be obtained by making ϵ complex.

The value of l and the length of the chord C are given by

$$l = a/(1+\epsilon), \tag{32}$$

$$C = 4l[1+\epsilon^2 l/(a+\epsilon l)]. \tag{33}$$

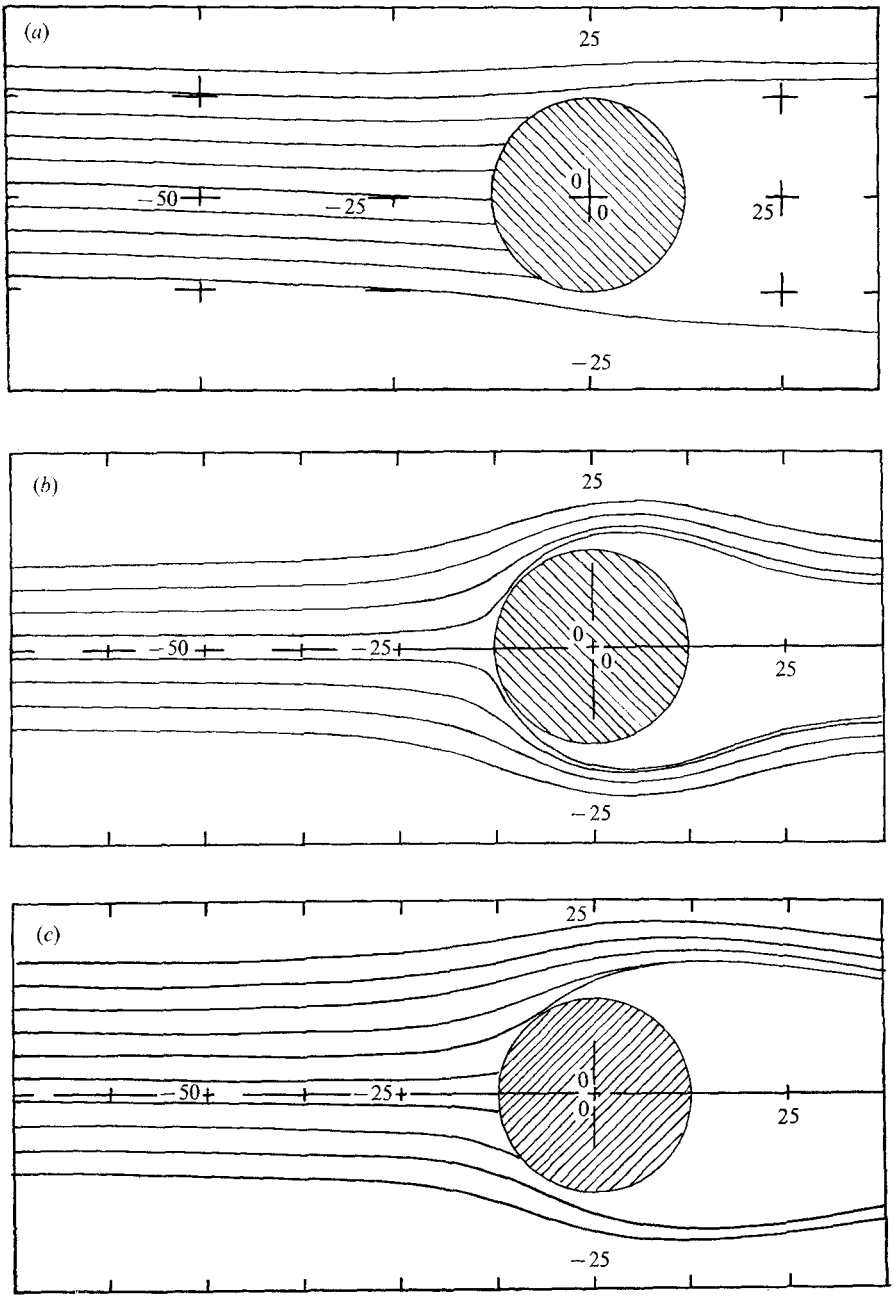

FIGURE 3. Particle trajectories in the vicinity of a circular cylinder. $U = 6$ m/s, $\rho_p = 1400$ kg/m^3. (*a*) $D_p = 100$ μm. (*b*) $D_p = 10$ μm. (*c*) $D_p = 20$ μm.

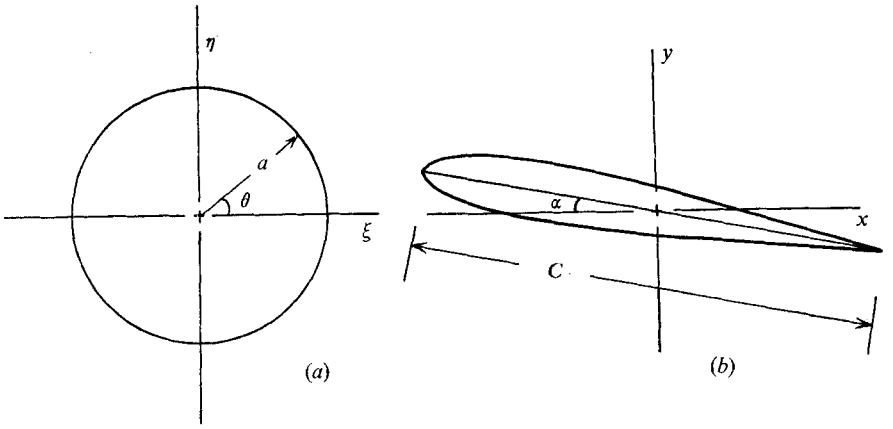

FIGURE 4. Transformation of a circle to a Joukowsky aerofoil.
(a) ζ plane. (b) Z plane.

The stream function ψ of a potential flow round a cylinder in the ζ plane is given by

$$\psi = U\eta[1-a^2/(\xi^2+\eta^2)], \tag{34}$$

where $\zeta = \xi + i\eta$. For the flow to leave the trailing edge of the aerofoil with finite velocity (the Kutta–Joukowsky condition) a circulation term has to be added to the above stream function, which becomes

$$\psi = U\eta\left(1-\frac{a^2}{\xi^2+\eta^2}\right)+K\log(\xi^2+\eta^2)^{\frac{1}{2}}. \tag{35}$$

From the above stream function the velocity components in the plane of the cylinder can be obtained; these are given by

$$U_\zeta = \frac{\partial\psi}{\partial\eta} = U\left\{1+\frac{a^2(\eta^2-\xi^2)}{(\xi^2+\eta^2)^2}+\frac{K\eta}{(\xi^2+\eta^2)}\right\}, \tag{36}$$

$$V_\zeta = -\frac{\partial\psi}{\partial\xi} = \frac{-2a^2U\xi\eta}{(\xi^2+\eta^2)^2}+\frac{K\xi}{(\xi^2+\eta^2)}. \tag{37}$$

The value of the circulation K which satisfies Kutta–Joukowsky condition in the case of a symmetrical aerofoil is given by

$$K = 2aU\sin\alpha. \tag{38}$$

The velocity components in the aerofoil plane can be obtained from the following relationship:

$$\frac{dw}{dz} = \frac{dw}{d\zeta}\frac{d\zeta}{dz}, \tag{39}$$

where w is the complex potential and equal to

$$w = \psi + i\phi; \tag{40}$$

the velocity components in the Z and ζ planes are given by

$$-U_z + iV_z = dw/dz, \tag{41}$$

$$-U_\zeta + iV_\zeta = dw/d\zeta. \tag{42}$$

By substituting the values of dw/dz and $dw/d\zeta$ from (41) and (42) into (9), differentiating (1) with respect to ζ and substituting the results into (39) a relationship between the velocity components in the aerofoil plane and those in the ζ plane can be obtained.

4.1. *The equations of motion of a particle near an aerofoil*

The equations of motion of a particle in the vicinity of an aerofoil are the same as those for the case of a cylinder. Equations (29) and (30) for the case of an aerofoil can be solved numerically if the values of U_g and V_g are known. To obtain the velocity components in the aerofoil plane the velocity components in the cylinder plane have to be calculated first. Therefore, a reversed transformation from the plane of the aerofoil, back to the plane of the cylinder is required. This can be done by reversing the transformation equation (31), i.e. by obtaining two relationships for ξ and η in terms of x and y. This reversed transformation gives four points (ζ, η) in the ζ plane which satisfy the transformation equation. The correct point is the one which falls in the corresponding quadrant and occupies a similar position relative to the cylinder. After determining the point in the plane of the cylinder, the velocity components U_ζ and V_ζ can be calculated from (36) and (37), and from (39), (41) and (42) the velocity components U_z and V_z can be obtained. Once the values of the velocity components are known the drag coefficient can be determined from (4). By substituting these values into (29) and (30) and solving numerically using the Runge–Kutta method, the velocity after a time dt can be obtained. By considering the particle to be moving with the average velocity the co-ordinate of the new position of the particle is obtained. At the new point the velocity of the air flow is unknown and the point has to be transformed back to the plane of the cylinder. A computer program has been written to carry out these calculations and to trace the particle trajectory, see figure 5.

Figure 6 (*a*) shows the particle trajectories for the case of an aerofoil transformed from a circle of radius $a = 12{\cdot}5$ mm by using (1) with $\epsilon = 0{\cdot}1$ and an angle of the incidence (of the aerofoil to the flow) $\alpha = 5°$. The particle parameters used are $D_p = 10\,\mu$m, $\rho_p = 1400\,\text{kg/m}^3$ and $U = 6$ m/s; the fluid is air. Figure 6 (*b*) shows the particle trajectory for the above case but with $\alpha = 15°$.

By putting $\epsilon = 0$ the circle is transformed to a flat plate, and the particle trajectories take the shapes shown in figures 7 (*a*) and (*b*). The particle parameters used in this case are $D_p = 10$ or $100\,\mu$m, $\rho_p = 1400\,\text{kg/m}^3$ and $U = 6$ m/s. Figures 8 (*a*) and (*b*) show the particle trajectories for the case given in figure 6, except that the particle diameter is taken to be $100\,\mu$m and the aerofoil is inclined at angles $\alpha = 0$ and 15° respectively. Also, figure 9 shows the particle trajectories in the case of an aerofoil for the following parameters: $\alpha = 5°$ or 15°, $\rho_p = 1400\,\text{kg/m}^3$, $U = 12$ m/s and $D_p = 10$ or $100\,\mu$m. In all these cases the particles were admitted at a distance of 75 mm.

4.2. *Discussion of results*

Figures 6 (*a*) and (*b*) show the effect of changing the incidence from 5° to 15° on a 12 % thick symmetrical Joukowsky aerofoil for an air speed of 6 m/s and particle size and density of $10\,\mu$m and $1400\,\text{kg/m}^3$ respectively. Owing to the fact that the

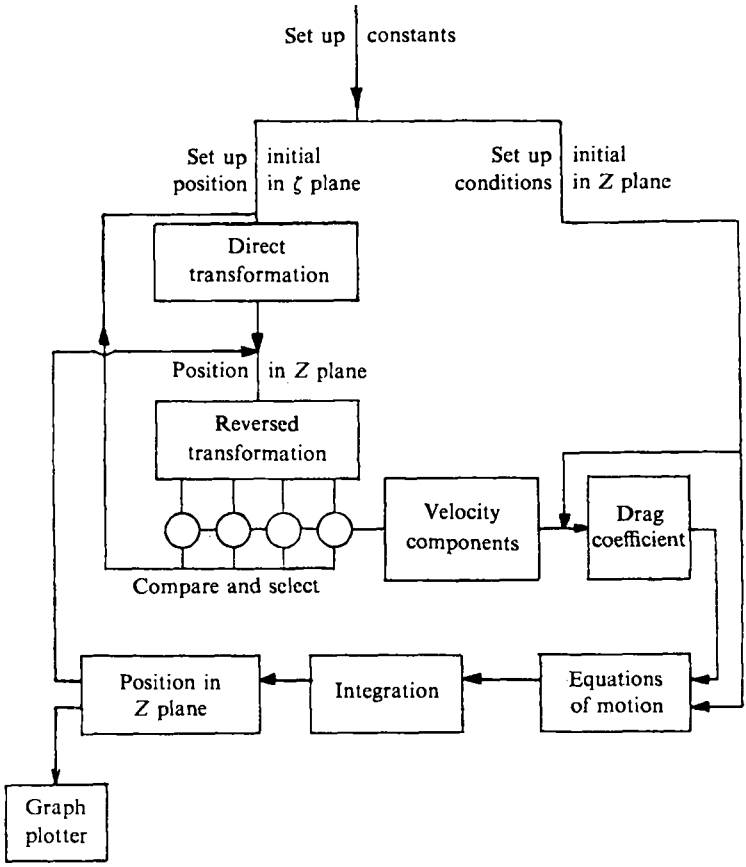

FIGURE 5. Flow diagram.

velocity field of the aerofoil causes particles which are initially outside the projected (vertical) area of the aerofoil to collide with it, the normal definition of collision efficiency as applied to a cylinder is not valid. In this case, therefore, we define the collision efficiency as the initial vertical area of the powder flow which collides with the aerofoil to the vertical projected area of the aerofoil. These efficiencies are 0·79 and 0·81 respectively for $\alpha = 5°$ and 15°. In the case of $\alpha = 15°$ a considerable displacement of the flow occurs.

Comparison of figures 6 (*b*) and 7 (*a*) shows the effect of thickness for $U = 6$ m/s, $\rho_p = 1400\,\mathrm{kg/m^3}$, $D_p = 10\,\mu\mathrm{m}$ and $\alpha = 15°$. The collision efficiency has increased to 0·93 for the flat-plate section. In figure 7 (*b*) the particle size is increased to $100\,\mu\mathrm{m}$ and the collision efficiency rises to 1·16. This increase in efficiency is due to the fact that fewer of the larger particles are deflected past the aerofoil by the velocity field near the aerofoil nose.

Figure 8 (*a*) shows the effect of gravity only, the aerofoil being at zero incidence. The collision efficiency is 0·92. At 15° incidence, see figure 8 (*b*), the efficiency rises to 1·10 and there is an indication from the particle paths that some concentration of deposits could be expected at the leading edge. A similar effect has been found experimentally by Parker & Ryley (1970).

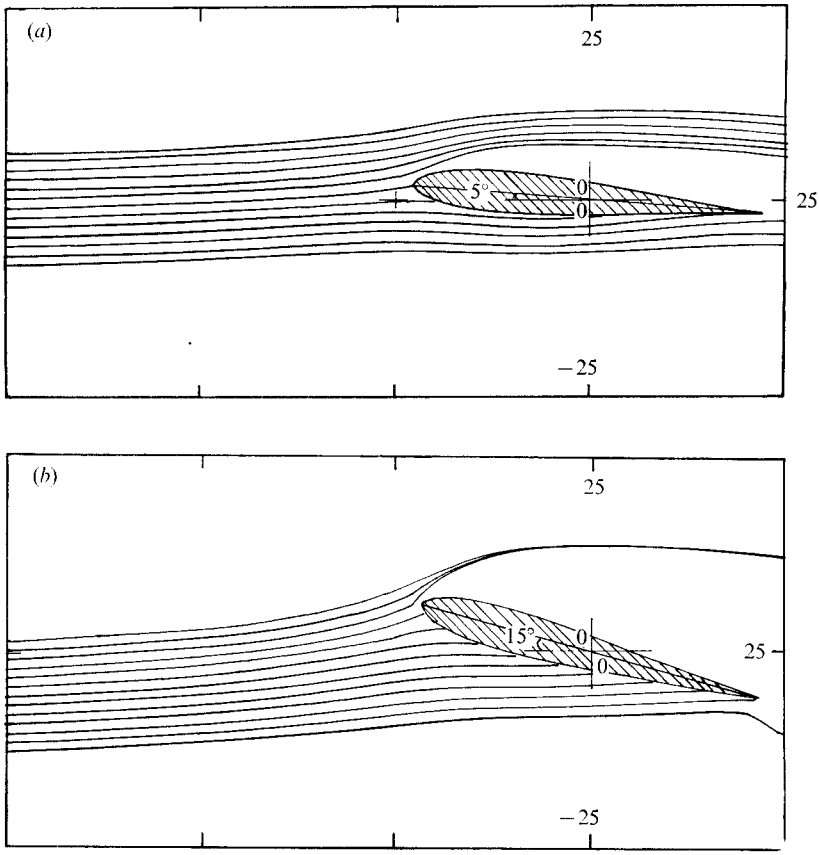

FIGURE 6. Particle trajectories near an aerofoil. $U = 6$ m/s, $D_p = 10$ μm, $\rho_p = 1400$ kg/m^3. (*a*) $\alpha = 5°$. (*b*) $\alpha = 15°$.

In figures 9(*a*)–(*d*) the air speed has been increased to 12 m/s with resultant particle efficiencies of 0·78, 1·09, 0·88 and 1·05 respectively. The collision efficiencies for the 10 μm particles, figures 9(*a*) and (*c*), have not changed significantly from the results at 6 m/s, i.e. 0·79 and 0·81, in figures 6(*a*) and (*b*). For the larger (100 μm) particles also the collision efficiency is the same at the two speeds.

5. Discussion and conclusions

5.1. *Response of powder particle to air flow*

From figure 2 it is seen that the accelerating length of a particle, from the point of its feed to the air stream, depends on the particle diameter and density and the velocity of air stream. Also, if this analysis is used for the case of dilute-phase transport in pipes, it is obvious that the accelerating length depends on the loading (W) as well. Therefore the accelerating length is a function of $U_g D_p \rho_p (W/g)$ for a given gas. Zenz (see Zenz & Othmer) suggested that the accelerating length is function of $W/\rho_g U_g$. These conclusions are near to each other, the difference being that the effect of Reynolds number appears in the first formula through the

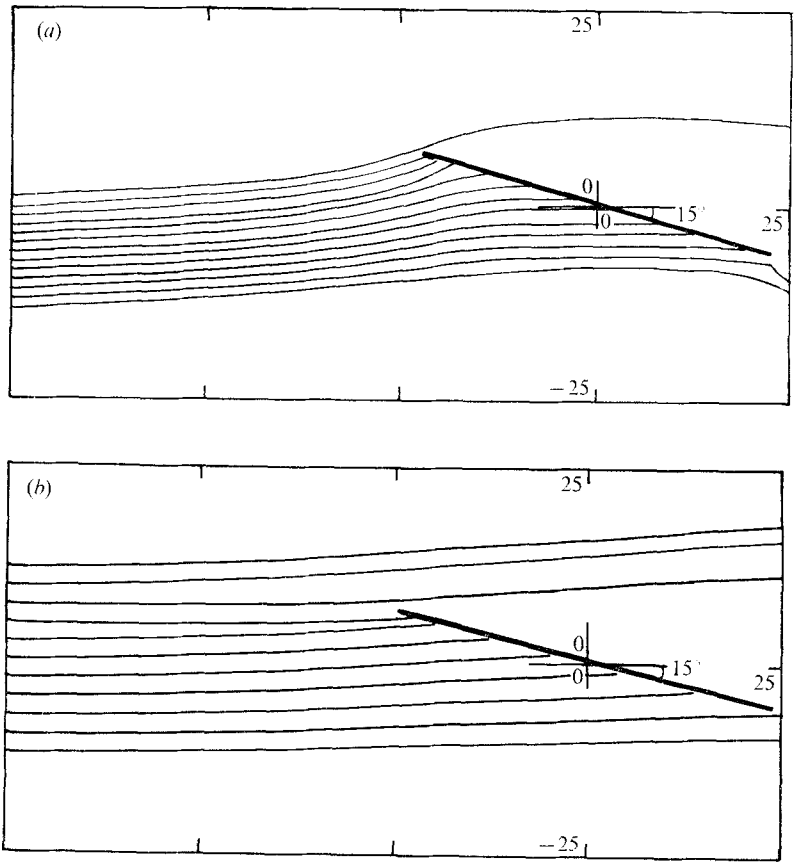

FIGURE 7. Particle trajectories near a flat plate. $\alpha = 15°$, $U = 6$ m/s, $\rho_p = 1400$ kg/m^3. (a) $D_p = 10\,\mu$m. (b) $D_p = 100\,\mu$m.

particle diameter, and through the fluid density in the second. However, in the second group if the loading is changed by changing the particles' density the accelerating length will change, contrary to the conclusion reached by Russ, Culgan & Hinkle. On the other hand in the first group the accelerating length does not change by changing the particles' density and hence the loading.

The case in which the particles material is Tenite, particle diameter = 2·5 mm, air velocity = 34·5 m/s and loading $W = 130$ kg/s m^2 has been solved using this analysis and it agrees exactly with the curve given by Hinkle for the above case and reported by Zenz & Othmer. *Loading* is defined here as the weight of the particle passing through a unit area.

5.2. *Collision of powder particles with a cylinder*

From figure 3(a) it is obvious that, owing to the effect of gravity, the particle trajectories are no longer symmetrical about the x axis and the possibility of collision with the upper half of the cylinder will be more than that in the lower half. Also, it can be deduced that the particle admitted at the point $(-75, 12{\cdot}5)$ will graze the cylinder, while it is the particle admitted at the point $(-75, -9)$

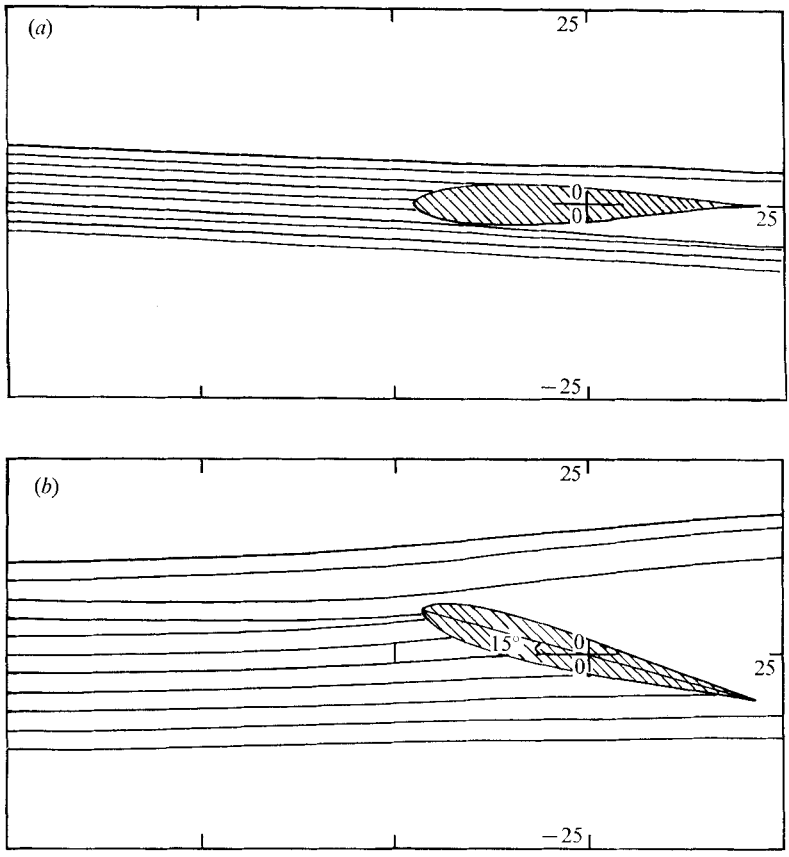

FIGURE 8. Particle trajectories near an aerofoil. $U = 6$ m/s, $D_p = 100$ μm, $\rho_p = 1400$ kg/m^3. (*a*) $\alpha = 0$. (*b*) $\alpha = 15°$.

in the lower half that will graze the cylinder. From this it can be concluded that the simplification of neglecting the effect of gravity is unjustified even in cases with particle diameter and density as low as 100 μm and 1400 kg/m^3 respectively.

From figure 3(*b*) it can be shown that the particles of small diameter (10 μm) will follow to some extent the air streamlines. Hence the particles will not collide with the cylinder except in the very small region which reaches the cylinder near the stagnation point.

On comparing these results with that of Michael (see Michael & Norey 1969) we find large differences. This is because Michael has assumed that the flow is a Stokes flow and the drag coefficient is $24/R_N$, which is far less than the experimental values when the Reynolds number exceeds 0·3. Furthermore, in case of large-diameter particles, the trajectories of the particles which do not collide with the cylinder spread away from the cylinder, while those of small-diameter particles converge towards the x axis. From the high-speed films taken for the case of the cylinder, it is apparent that the trajectories of the large particles do spread after passing the cylinder, while the small-diameter particles converge to form vortices behind the cylinder.

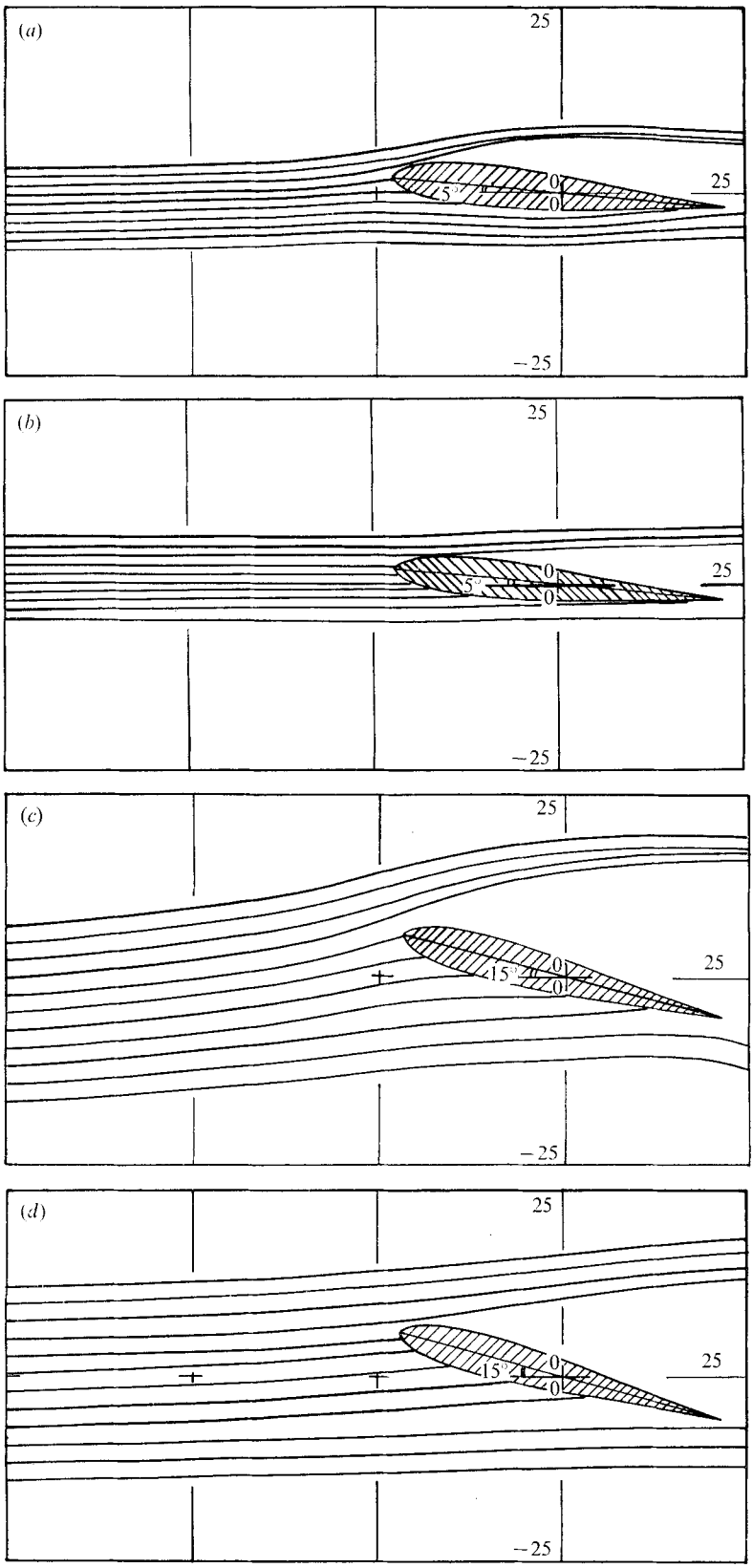

FIGURE 9. Particle trajectories near an aerofoil. $U = 12$ m/s, $\rho_p = 1400$ kg/m^3. (*a*) $\alpha = 5°$, $D_p = 10\,\mu$m. (*b*) $\alpha = 5°$, $D_p = 100\,\mu$m. (*c*) $\alpha = 15°$, $D_p = 10\,\mu$m. (*d*) $\alpha = 15°$, $D_p = 100\,\mu$m.

5.3. *Collision of particles with an aerofoil*

The effects of particle size and density, the airspeed, aerofoil thickness and incidence on particle trajectories in the vicinity of the lifting aerofoil have been studied and the following general conclusions obtained.

(i) The effect of aerofoil thickness on the collision efficiency is not large ($\sim 10\,\%$) at high ($\simeq 15°$) incidence. This indicates that the aerodynamic (lift) effect predominates over the thickness effect. However, at very small angles of incidence ($\simeq 0$) a larger number of particles in a given flow will collide with the thicker section although the collision efficiency may not be greatly changed.

(ii) Smaller particles are affected by the aerofoil velocity field to a much larger extent than the large particles and tend to follow the streamlines more closely. Practically, this would result in higher collision efficiencies for larger particles in any given situation because fewer particles are deflected past the aerofoil nose by the upward velocities due to lift. If the lift is small (low incidence) the effects of gravity could modify this conclusion.

(iii) There is evidence in some cases that concentration of particles can be expected to occur near the leading and trailing edges. This is supported by some experimental results.

(iv) When the air speed was increased from 6 to 12 m/s there was very little change in the collision efficiency for either the small (10 μm) particles or the larger (100 μm) particles. Thus for a lifting body the trend is rather different from the case of particle collision with a non-lifting body, for which, in general, the collision efficiency rises with speed.

Appendix

The drag coefficient equations used are

$$C_d = 24{\cdot}0/R_N \quad \text{for} \quad R_N < 0{\cdot}1,$$

$$C_d = 22{\cdot}73/R_N + 0{\cdot}0903/R_N^2 + 3{\cdot}69 \quad \text{for} \quad 0{\cdot}1 < R_N < 1{\cdot}0,$$

$$C_d = 29{\cdot}1667/R_N - 3{\cdot}8889/R_N^2 + 1{\cdot}222 \quad \text{for} \quad 1{\cdot}0 < R_N < 10{\cdot}0,$$

$$C_d = 46{\cdot}5/R_N - 116{\cdot}67/R_N^2 + 0{\cdot}6167 \quad \text{for} \quad 10{\cdot}0 < R_N < 100{\cdot}0,$$

$$C_d = 98{\cdot}33/R_N - 2778/R_N^2 + 0{\cdot}3644 \quad \text{for} \quad 100{\cdot}0 < R_N < 1000{\cdot}0,$$

$$C_d = 148{\cdot}62/R_N - 4{\cdot}75 \times 10^4/R_N^2 + 0{\cdot}357 \quad \text{for} \quad 1000{\cdot}0 < R_N < 5000{\cdot}0,$$

$$C_d = -490{\cdot}546/R_N + 57{\cdot}87 \times 10^4/R_N^2 + 0{\cdot}46 \quad \text{for} \quad 5000{\cdot}0 < R_N < 10000{\cdot}0,$$

$$C_d = -1662{\cdot}5/R_N + 5{\cdot}4167 \times 10^6/R_N^2 + 0{\cdot}5191 \quad \text{for} \quad 10000{\cdot}0 < R_N < 50000{\cdot}0.$$

REFERENCES

LANGMIUR, I. & BLODGETT, K. B. 1946 *Army–Air Force Rep.* no. 5418.

MARTLEW, D. L. 1960 The distribution of impact particles of various sizes on the blades of a turbine cascade. *Symposium Aerodynamic Capture of Particles.* Pergamon.

MICHAEL, D. H. & NOREY, P. W. 1969 Particle collision efficiencies for a sphere. *J. Fluid Mech.* **37**, 565.

NEILSON, J. H. & GILCHRIST, A. 1968 An analytical and experimental investigation of the velocities of particles entrained by the gas flow in nozzles. *J. Fluid Mech.* **33**, 131.

PARKER, G. J. & RYLEY, D. J. 1970 Equipment and techniques for studying the desposition of sub-micron particles on turbine blades. *Proc. Inst. Mech. Eng.* **184** (3*c*).

SAFFMAN, P. G. 1965 The lift on a small sphere in a slow shear flow. *J. Fluid Mech.* **22**, 285.

ZENZ, F. & OTHMER, O. 1960 *Fluidization and Fluid-Particle Systems.* Reinhold Publishing Co.